Pansharpening With Spatial Framelet Consistency and Spectral Gradient Low Rank Priors

Penghao Yin*, Jinchao Li*, and Yongyong Chen‡

***Abstract*—Pansharpening entails the fusion of a low spatial-resolution spectral (LRMS) image with a high-resolution gray-scaled panchromatic (PAN) image to produce a high spatial-resolution spectral (HRMS) image. In traditional models, spectral consistency terms such as nuclear norm and total-variation (TV) will cause excessive calculating complexity and flaws like staircase artifacts. To solve these problems, we propose a novel pansharpening model with spatial framelet consistency and spectral gradient low rank priors (SFLR). Leveraging the similarity between HRMS and PAN in framelet space, we introduce a spatial framelet consistency term. Additionally, as each slice of ground-truth HRMS image is similar, the spectral gradient tensor of HRMS will be sparse. So we employ the spectral gradient low rank prior to preserve the low-rank characteristics of HRMS. The model is solved using the alternating direction method of multipliers (ADMM) framework. Experimental results on a reduced dataset demonstrate that our model surpasses many traditional methods but falls short compared to certain modern approaches.**

***Index Terms*—Pansharpening, framelet, spectral gradient low rank, alternating direction method of multipliers (ADMM).**

I. Introduction

HIGH-RESOLUTION multispectral (HRMS) remote sensing images serve as a fundamental component in various practical applications, including change detection [1], target recognition [2] , and classification [3]. Due to inherent limitations in signal-to-noise ratio [4], numerous satellite-based sensors, such as Gaofen-2 (GF-2), QuickBird (QB), and WorldView-3 (WV-3), capture low spatial-resolution multispectral (LRMS) images alongside gray-scaled panchromatic (PAN) images with higher spatial information using separate sensors. Pansharpening involves integrating spatial and spectral information from the LRMS image and its corresponding PAN image to produce a refined HRMS image. Fig 1 illustrates the process of our method SFLR.

Researchers have developed many different methodologies for pansharpening. The popular pansharpening methods can be divided into several types, including CS (component substitution), MRA (multi-resolution analysis), DL (deep learning) and VO (variational optimization).

In CS methods, the LRMS image's spatial aspect is separated using spectral transformation and substituted with the PAN image. While CS-based methods are often preferred for their decreased computational workload, they frequently introduce significant spectral alterations. Famous CS methods mainly include the principal component analysis (PCA) [5] method, the intensity-hue-saturation (IHS) [6] method, the Gram-Schmidt adaptive (GSA) [7] method, the band-dependent spatial-detail (BDSD) [8] method, and the partial replacement adaptive component substitution (PRACS) [9] method.

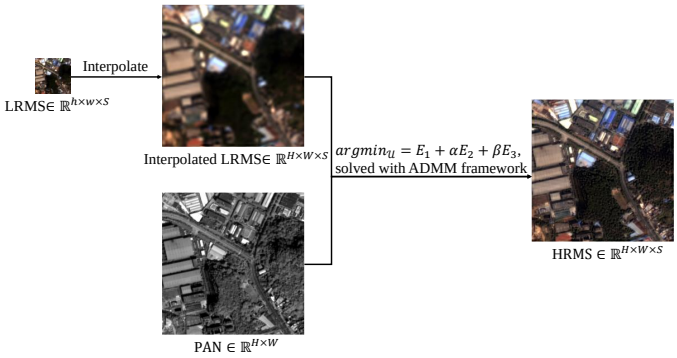

Fig. 1. The process of SFLR.

In MRA methods, spatial information derived from the PAN image is injected into the upsampled LRMS image through multi-scale decomposition. These kind of methods exhibit enhanced spectral coherence but may sacrifice spatial fidelity. In general, both CS and MRA methods demonstrate robustness across various datasets. Additionally, they typically entail minimal parameter tuning and possess lower computational demands. Consequently, these approaches are frequently employed as benchmarks in the field of pansharpening. Famous MRA methods mainly include the "a-trous" wavelet transform (ATWT) [10] method, the additive wavelet luminance proportional (AWLP) [11] method, and the smoothing filter-based intensity modulation (SFIM) [12] method.

Recently, deep learning (DL) has been increasingly popular. Many convolutional neural network (CNN)-based approaches, e.g., [13], [14], [15], [16], [17], [18], have been designed for pansharpening. These methods demonstrate outstanding abilities in feature extraction and learning nonlinear mappings, surpassing conventional approaches in performance. Nevertheless, CNN-based techniques often demand substantial computational resources and extensive training data, greatly constraining their computational efficiency, generalization capability, and interpretability of models.

Variational optimization approaches lie between the CS/MRA and CNN-based techniques, typically striking a

Penghao Yin ,Jinchao Li are with the School of Science, Harbin Institute of Technology, Shenzhen, Guangdong 518055, China (e-mail: phyin2024@gmail.com; 210810626@stu.hit.edu.cn).

Yongyong Chen is with the School of Computer Science and Technology, Harbin Institute of Technology, Shenzhen, Guangdong 518055, China (e-mail: cyy2020@hit.edu.cn).

*:Equal Contribution.

balance between effectiveness and computational efficiency. These methods are distinguished by their strong generalization capabilities and the interpretability of the resulting models. These methods, e.g., [19], [20], [21], [22], [23], [24], [25], [26], consider the pansharpening problem as an ill-posed optimization problem, which is related to LRMS image, PAN image, and fuded HRMS image. By employing the conventional image super-resolution (ISR) degradation model, users can obtain promising resuts, particularly when accounting for the traits of MS sensors. Nonetheless, because of the intertwining nature of the poorly defined blurring and downsampling issues, numerous super-resolution models either demonstrate excessive complexity in resolving them independently, or yield a perplexing amalgamation of unfolding-based and tensor-based approaches.

In this report, we propose a novel VO-based pansharpening method, i.e., the spatial framelet consistency and spectral gradient low rank priors-based framework, called SFLR. Our model mainly consists of 3 folds. Firstly, according to the spectral consistency between the low-pass filtered, or blurred HRMS and the interpolated LRMS image, we construct the spectral fidelity term. Secondly, inspired by the similarity between the framelet-transformed HRMS image and the histogram-matched copied PAN image 3, we formulate the spatial framelet consistency prior. As pansharpening is an ill-posed problem, we introduce a low-rank gradient nuclear norm prior to this model, which ensures the unique solution. Under the popular alternating direction method of multipliers (ADMM) framework, the optimization problem is efficiently solved. Experiments has shown the advantages of SFLR compared with some traditional methods, but it has also shown the insufficiency compared with some novel models.

The contributions of this report are summarized as follows:

• We innovatively design a spatial framelet consistency prior to replace traditional spatial consistency priors. Such a prior is based on our statistical analysis which proves the similarity between blurred HRMS and the interpolated LRMS image. It improves the accuracy of pansharpening.

• We utilize the low rank property of the spectral gradient of HRMS, and we raise the spectral gradient low rank prior for pansharpening.

• We consequently build a novel pansharpening model with spatial framelet consistency and spectral gradient low rank priors. Then the ADMM method is utilized for solving the proposed model.

The remainder of this report are as follows. Section II gives the notations and preliminaries of this report. Section III introduces the SFLR model. Section IV introduces its optimization algorithm. Section V performs the experiments. Section VI concludes this report and introduces the following work.

II. Pansharpening with Spatial Framelet Consistency and Spectral Gradient Low Rank Priors

In this section, the proposed model is constructed by three important priors. At the beginning of this part, the important notations are listed in table I.

TABLE I
NOTATIONS AND ITS EXPLANATIONS

Notations	Explanations
$\mathcal{U} \in \mathbb{R}^{H\times W\times S}$	HRMS image with size $H \times W \times S$
$\mathcal{M} \in \mathbb{R}^{h\times w\times S}$	LRMS image with size $h \times w \times S$
$\mathbf{p} \in \mathbb{R}^{H\times W}$	PAN image with size $H \times W$
$\mathcal{P} = \{\mathbf{p}, \cdots, \mathbf{p}\} \in \mathbb{R}^{H\times W\times S}$	Duplicated PAN image with size $H \times W \times S$
$\mathcal{U}_{i,j,k}$	i^{th} row, j^{th} column, k^{th} band of $\mathcal{U}$
$\|\mathcal{U}\|_F = \sqrt{\sum_{i,j,k} \|\mathcal{U}_{i,j,k}\|^2}$	Frobenius norm
$\|\mathcal{U}\|_p = (\sum_{i,j,k} \|\mathcal{U}_{i,j,k}\|^p)^{\frac{1}{p}}$	l_p norm
$\|\mathcal{U}\|_*$	Nuclear norm
$(\cdot)^T$	Transpose of $(\cdot)$

A. Spectral Consistency Term

Generally, LRMS image $\mathcal{M}$ can be regarded as degradation of HRMS image $\mathcal{U}$, so there are equation as follows:

$$\mathcal{M} = (\mathcal{U} * \mathcal{S}) \downarrow_r + \mathcal{N}_0, \tag{1}$$

where $*$ means t-Conv operator, $\downarrow_r$ is downsampling operator with the scale factor r, and $\mathcal{N}_0$ is an additional zero-mean Gaussian noise.

Upsampling both sides of the equation simultaneously, the equation can be reformed as follows:

$$\mathcal{M} \uparrow_r = \mathcal{U} * \mathcal{S} + \mathcal{N}_1, \tag{2}$$

where $\mathcal{N}_1$ is also an additional zero-mean Gaussian noise.

According to the equation above, we propose the spectral consistency term E_1 as follows:

$$E_1 = \|\mathcal{U} * \mathcal{S} - \mathcal{M}_{itp}\|_F, \tag{3}$$

where $\mathcal{M}_{itp}$ is the tensor obtained by cubic spline interpolation of $\mathcal{M}$.

B. Spatial Framelet Consistency Term

The framelet regularization has been effectively applied to a lot of image processing fields, such as image deblurring [27], tensor completion [28], and image destriping [29]. Motivated by its powerful usage, we make some numerical experiments to prove the similarity between HRMS and histogram-matched PAN. Fig. 2 shows the selected HRMS and PAN as an example, and Fig. 3 depicts their distribution and their difference's distribution.

The figure points out that the HRMS image and the histogram-matched PAN image are similar to each other. According to this result, we propose the spatial framelet consistency term as follows:

$$E_2 = \|W(L\mathcal{U} - L\mathcal{P}_{his})\|_F, \tag{4}$$

where L is a reshaping operator which turns a tensor with size $\mathbb{R}^{H\times W\times S}$ into the tensor with size $\mathbb{R}^{S\times HW}$, and $\mathcal{P}_his$ is the image matched to $\mathcal{P}$ based on the histogram of $\mathcal{M}$.

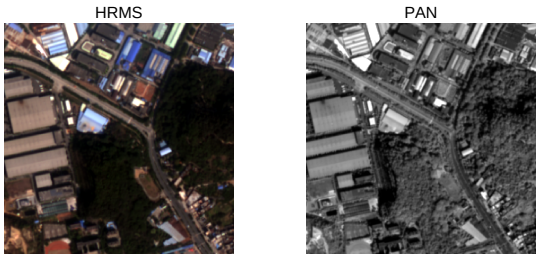

Fig. 2. The selected HRMS and PAN.

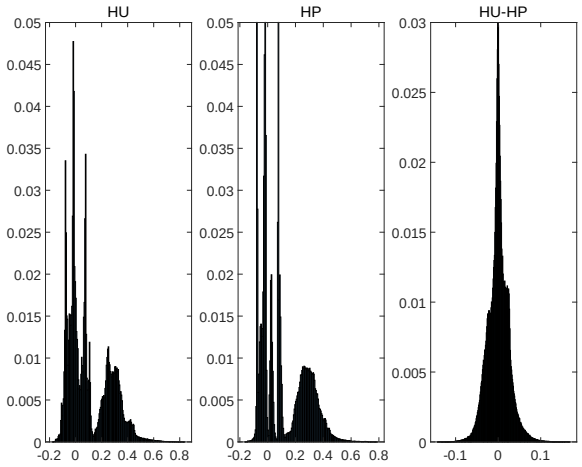

Fig. 3. The histograms of $W(L\mathcal{U})$, $W(L\mathcal{P})$ and$W(L\mathcal{U}-L\mathcal{P})$, where $\mathcal{U}$ and $\mathcal{P}$ are selected HRMS and histogram-matched PAN respectively.

C. Spectral Gradient Low Rank Prior

[30] points out the low-rank characteristic of $\mathcal{U}$'s spectral gradient. According to this paper, we construct the spectral gradient low rank prior as follows:

$$E_3 = \|L\nabla_z\mathcal{U}\|_*, \tag{5}$$

where $L\nabla_z\mathcal{U}$ means $[vec(\mathcal{U}_{,,2}-\mathcal{U}_{,,1})^T,\cdots,vec(\mathcal{U}_{,,S}-\mathcal{U}_{,,S-1})^T,-vec(\mathcal{U}_{,,1}\})^T]^T$.

We introduce matrix A as follows:

$$A=\begin{bmatrix}-1&1&0&0&\cdots&0&0\\0&-1&1&0&\cdots&0&0\\0&0&-1&1&\cdots&0&0\\0&0&0&-1&\cdots&0&0\\\vdots&\vdots&\vdots&\vdots&\ddots&\vdots&\vdots\\0&0&0&0&\cdots&-1&1\\0&0&0&0&\cdots&0&-1\end{bmatrix}_{b\times b}, \tag{6}$$

equation 5 can be rewritten as follows:

$$E_3 = \|A(L\mathcal{U})\|_*, \tag{7}$$

D. SFLR

By taking the weighted sum of E_1, E_2 and E_3, we can construct the novel model pansharpening with spatial framelet consistency and spectral gradient low rank priors (SFLR) as

$$\arg\min_U \frac{1}{2}\|\mathcal{U}*\mathcal{S}-\mathcal{M}_{itp}\|_F^2+\alpha\|W(L\mathcal{U}-L\mathcal{P}_{his})\|_1 + \beta\|L\nabla_z\mathcal{U}\|_*, \tag{8}$$

where α and β are non-negative adjustable scalars.

III. Solution Algorithm

By introducing auxiliary variables $\mathcal{U}_1=\mathcal{U},\mathcal{U}_2=\mathcal{U},G=W(L\mathcal{U}_1-L\mathcal{P}),B=L\nabla_z\mathcal{U}_2$, equation 8 can be rewritten as

$$\begin{aligned}&\arg\min_U \frac{1}{2}\|\mathcal{U}*\mathcal{S}-\mathcal{M}_{itp}\|_F^2+\alpha\|W(L\mathcal{U}-L\mathcal{P}_{his})\|_1 + \beta\|L\nabla_z\mathcal{U}\|_*,\\ &s.t.\ \mathcal{U}_1=\mathcal{U},\mathcal{U}_2=\mathcal{U},G=W(L\mathcal{U}_1-L\mathcal{P}_{his}),B=L\nabla_z\mathcal{U}_2.\end{aligned} \tag{9}$$

The augmented Lagrange function is constructed as

$$\begin{aligned}F(\mathcal{U},\mathcal{U}_1,\mathcal{U}_2,G,B,\Lambda_1,\Lambda_2,\Lambda_3,\Lambda_4)&=\frac{1}{2}\|\mathcal{U}*\mathcal{S}-\mathcal{M}_{itp}\|_F^2\\ &+\alpha\|G\|_1+\beta\|B\|_*+\frac{\gamma_1}{2}\|\mathcal{U}_1-\mathcal{U}+\Lambda_1\|_F^2\\ &+\frac{\gamma_2}{2}\|\mathcal{U}_2-\mathcal{U}+\Lambda_2\|_F^2+\frac{\gamma_3}{2}\|G-W(L\mathcal{U}_1-L\mathcal{P}_{his})+\Lambda_3\|_F^2\\ &+\frac{\gamma_4}{2}\|B-L\nabla_z\mathcal{U}_2+\Lambda_4\|_F^2,\end{aligned} \tag{10}$$

where $\Lambda_1,\Lambda_2,\Lambda_3,\Lambda_4$ are scaled lagrangian multipliers, $\alpha,\beta,\gamma_1,\gamma_2,\gamma_3,\gamma_4>0$.

According to ADMM, model 10 can be solved by solving following subproblems.

A. Optimization of $\mathcal{U}_1$

According to model 10, the $\mathcal{U}_1$ sub-problem is as follows:

$$\begin{aligned}\mathcal{U}_1^{(k+1)}=\arg\min_{\mathcal{U}_1}&\frac{\gamma_1}{2}\|\mathcal{U}_1-\mathcal{U}+\Lambda_1\|_F^2\\ &+\frac{\gamma_3}{2}\|G-W(L\mathcal{U}_1-L\mathcal{P}_{his})+\Lambda_3\|_F^2.\end{aligned} \tag{11}$$

As $\|(\cdot)\|_F$ is equal to $\|L(\cdot)\|_F$, the sub-problem can be rewritten as

$$\begin{aligned}\mathcal{U}_1^{(k+1)}=\arg\min_{\mathcal{U}_1}&\frac{\gamma_1}{2}\|L\mathcal{U}_1-L\mathcal{U}+L\Lambda_1\|_F^2\\ &+\frac{\gamma_3}{2}\|WL\mathcal{U}_1-G-WL\mathcal{P}_{his}-\Lambda_3\|_F^2.\end{aligned} \tag{12}$$

Take the derivative of both sides of the equation with respect to $\mathcal{U}_1$, we get

$$\gamma_1(L\mathcal{U}_1 - L\mathcal{U} + L\Lambda_1) + \gamma_3 W^T(WL\mathcal{U}_1 - G - WL\mathcal{P}_{his} - \Lambda_3) = 0 \quad (13)$$

As $W^TW = I$, the equation can be rewritten as

$$(\gamma_1+\gamma_3)L\mathcal{U}_1 = \gamma_1(L\mathcal{U} - L\Lambda_1) + \gamma_3 W^T(G + WL\mathcal{P}_{his} + \Lambda_3), \quad (14)$$

$$L\mathcal{U}_1 = \frac{1}{(\gamma_1+\gamma_3)}(\gamma_1(L\mathcal{U} - L\Lambda_1) + \gamma_3 W^T(G + WL\mathcal{P}_{his} + \Lambda_3). \quad (15)$$

After getting $L\mathcal{U}_1$, we can obtain $\mathcal{U}_1^{(k+1)}$ by

$$\mathcal{U}_1^{(k+1)} = L^{-1}L\mathcal{U}_1. \quad (16)$$

B. Optimization of $\mathcal{U}_2$

According to model 10, the $\mathcal{U}_2$ sub-problem is as follows:

$$\mathcal{U}_2^{(k+1)} = \arg\min_{\mathcal{U}_2} \frac{\gamma_2}{2}\|\mathcal{U}_2 - \mathcal{U} + \Lambda_2\|_F^2 + \frac{\gamma_4}{2}\|B - L\nabla_z\mathcal{U}_2 + \Lambda_4\|_F^2. \quad (17)$$

The sub-problem can also be rewritten as

$$\mathcal{U}_2^{(k+1)} = \arg\min_{\mathcal{U}_2} \frac{\gamma_2}{2}\|L\mathcal{U}_2 - L\mathcal{U} + L\Lambda_2\|_F^2 \quad (18)$$

$$+\frac{\gamma_4}{2}\|AL\mathcal{U}_2 - B - \Lambda_4\|_F^2. \quad (19)$$

Take the derivative of both sides of the equation with respect to $\mathcal{U}_2$, we get

$$\gamma_2(L\mathcal{U}_2 - L\mathcal{U} + L\Lambda_2) + \gamma_4 A^T(AL\mathcal{U}_2 - B - \Lambda_4) = 0, \quad (20)$$

$$(\gamma_2 I + \gamma_4 A^TA)L\mathcal{U}_2 = \gamma_2(L\mathcal{U} - L\Lambda_2) + \gamma_4 A^T(B + \Lambda_4), \quad (21)$$

$$L\mathcal{U}_2 = (\gamma_2 I + \gamma_4 A^TA)^{-1}(\gamma_2(L\mathcal{U} - L\Lambda_2) + \gamma_4 A^T(B + \Lambda_4)). \quad (22)$$

After getting $L\mathcal{U}_2$, we can obtain $\mathcal{U}_2^{(k+1)}$ by

$$\mathcal{U}_2^{(k+1)} = L^{-1}L\mathcal{U}_2. \quad (23)$$

C. Optimization of G

According to model 10, the G sub-problem is as follows:

$$\alpha\|G\|_1 + \frac{\gamma_3}{2}\|G - W(L\mathcal{U}_1 - L\mathcal{P}_{his}) + \Lambda_3\|_F^2 \quad (24)$$

By using generalized-soft-thresholding scheme [31], we can solve the equation as follows:

$$G^{(k+1)} = \Psi_{\frac{\alpha}{\gamma_3}}(W(L\mathcal{U}_1 - L\mathcal{P}_{his}) - \Lambda_3). \quad (25)$$

D. Optimization of B

According to model 10, the B sub-problem is as follows:

$$B^{(k+1)} = \arg\min_B \beta\|B\|_* + \frac{\gamma_4}{2}\|B - L\nabla_z\mathcal{U}_2 + \Lambda_4\|_F^2, \quad (26)$$

By using singular-value-shrinkage method [32], we can solve the equation as follows:

$$B^{(k+1)} = QD_{\frac{\beta}{\gamma_4}}(\Sigma)V^T, \quad (27)$$

where $Q\Sigma V^T$ is the singular value decomposition of $L\nabla_z\mathcal{U}_2 - \Lambda_4$, $D_{\frac{\beta}{\gamma_4}}(\Sigma) = diag\{\max(\sigma_t - \frac{\beta}{\gamma_4}, 0)\}_{t\times t}$, and $\{\sigma_t\}_{t=1}^b$ are the singular values of $L\nabla_z\mathcal{U}_2 - \Lambda_4$.

E. Optimization of $\mathcal{U}$

According to model 10, the $\mathcal{U}$ sub-problem is as follows:

$$\mathcal{U}^{(k+1)} = \frac{1}{2}\|\mathcal{U} * \mathcal{S} - \mathcal{M}_{itp}\|_F^2 + \frac{\gamma_1}{2}\|\mathcal{U}_1 - \mathcal{U} + \Lambda_1\|_F^2 + \frac{\gamma_2}{2}\|\mathcal{U}_2 - \mathcal{U} + \Lambda_2\|_F^2, \quad (28)$$

which can be rewritten as

$$\mathcal{U}_{,,i}^{(k+1)} = \frac{1}{2}\left\|\mathcal{U}_{,,i} * \mathcal{S}_{,,i} - \mathcal{M}_{itp_{,,i}}\right\|_F^2 + \frac{\gamma_1}{2}\left\|\mathcal{U}_{1_{,,i}} - \mathcal{U}_{,,i} + \Lambda_{1_{,,i}}\right\|_F^2 + \frac{\gamma_2}{2}\left\|\mathcal{U}_{2_{,,i}} - \mathcal{U}_{,,i} + \Lambda_{2_{,,i}}\right\|_F^2, \quad (29)$$

where $(\cdot)^{(i)}$ is the i^{th} slice of tensor $(\cdot)$, $1 \le i \le S$.

We set that

$$\Sigma_{1_{,,i}} = F(S_{,,i})^{\ddagger} \cdot F(S_{,,i}) + \gamma_1 + \gamma_2, \quad (30)$$

$$\Sigma_{2_{,,i}} = F(S_{,,i})^{\ddagger} \cdot F(M_{,,i}) + \gamma_1(F(\mathcal{U}_{1_{,,i}}) + F(\Lambda_{1_{,,i}})) + \gamma_2(F(\mathcal{U}_{2_{,,i}}) + F(\Lambda_{2_{,,i}})), \quad (31)$$

so the solution of this sub-problem is given by

$$F(\mathcal{U}_{,,i}) = \Sigma_{2_{,,i}}./\Sigma_{1_{,,i}}, \quad (32)$$

$$\mathcal{U}_{,,i}^{(k+1)} = F^{-1}(\Sigma_{2_{,,i}}./\Sigma_{1_{,,i}}). \quad (33)$$

F. Optimization of $\Lambda_1, \Lambda_2, \Lambda_3$ and Λ_4

According to the ADMM framework, the Lagrangian multipliers $\Lambda_1, \Lambda_2, \Lambda_3$ and Λ_4 can be directly updated by

$$\Lambda_1^{(k+1)} = \Lambda_1 + \mathcal{U}_1 - \mathcal{U}, \quad (34)$$

$$\Lambda_2^{(k+1)} = \Lambda_2 + \mathcal{U}_2 - \mathcal{U}, \quad (35)$$

$$\Lambda_3^{(k+1)} = \Lambda_3 + G - W(L\mathcal{U}_1 - L\mathcal{P}_{his}), \quad (36)$$

$$\Lambda_4^{(k+1)} = \Lambda_4 + B - L\nabla_z\mathcal{U}_2. \quad (37)$$

The solution algorithm can be concluded in Algorithm 1.

Algorithm 1: The SFLR Algorithm

Input: $\mathcal{M}_{itp}, \mathcal{P}_{his}$

Initialization: Set $\alpha, \beta, \gamma_1, \gamma_2, \gamma_3, \gamma_4, \mathcal{S}, Iter = 200, k = 0, \epsilon = 2 \times 10^{-5}, \mathcal{U}^{(0)}, \mathcal{U}_1^{(0)}, \mathcal{U}_2^{(0)}, G^{(0)}, B^{(0)}, \Lambda_1^{(0)} = 0, \Lambda_2^{(0)} = 0, \Lambda_3^{(0)} = 0, \Lambda_4^{(0)} = 0$

for $k \leftarrow 0$ **to** $Iter - 1$ **do**

  Solve $\mathcal{U}_1^{(k+1)}$ via Eqn. 16;

  Solve $\mathcal{U}_2^{(k+1)}$ via Eqn. 23;

  Solve $G^{(k+1)}$ via Eqn. 25;

  Solve $B^{(k+1)}$ via Eqn. 27;

  Solve $\mathcal{U}^{(k+1)}$ via Eqn. 33;

  Update $\Lambda_1^{(k+1)}, \Lambda_2^{(k+1)}, \Lambda_3^{(k+1)}$ and $\Lambda_4^{(k+1)}$ via Eqn. 34,35,36,37;

  end if $\left\|\mathcal{U}^{(k+1)} - \mathcal{U}^{(k)}\right\|_F / \left\|\mathcal{U}^{(k)}\right\|_F < \epsilon$

end

Output: HRMS $\mathcal{U} = \mathcal{U}^{(k)}$

IV. EXPERIMENT

A. Setting

In OUR experiment, the Guangzhou dataset on reduced resolution is utilized for assessing the proposed SFLR approach. The Wald's protocol [33] is employed to make the reduced resolution data experiment, where the full resolution PAN and LRMS are filtered by sensors' modulation transfer functions (MTFs) and down-sampled by the resolution-ratio of 4 to produce the reduced resolution PAN and LRMS. Moreover, a polynomial kernel with 23 coefficients (EXP) [1] is employed to get the up-sampled LRMS image in the experiments.

Our model is compared with EXP [34], PRACS [35], BDSD_PC [36], AWLP [37], MF_HG [38], GLP-FS [39], C-GLP-R [40], LGC-P [41], WTVGlp [42], CDIF [43], NC-FSRM [44]. Meanwhile, we use peak signal-to-noise ratio (PSNR), structural similarity (SSIM), spectral angle mapper (SAM), spatial correlation coefficient (SCC), erreur relative global adimensionnelle de synthese (ERGAS) and Q4 to judge the quality of output images.

For parameters, we set $\alpha = 6.8 \times 10^2, \beta = 6.7 \times 10^3, \gamma_1 = 1.8 \times 10^{-4}, \gamma_2 = 5.0 \times 10^{-5}, \gamma_3 = 7.5 \times 10^{-4}, \gamma_4 = 5.0 \times 10^{-2}$.

B. Result Analysis

Using the settings above, we get the fusion images as Fig. 4, and the residuals as Fig. 5. The image and residual of ground truth is shown as Fig. 6. The numerical results are shown in table II.

According to Fig. 4 and Fig. 6, it is shown that the fusion result of our method is slightly lighter in the spectrum, and in terms of spatial dimension, it is blurrier than ground truth. According to table II, our method is better than a lot of traditional pansharpening methods. However, it is still worse than modern methods such as CDIF and NC-FSRM. So it still needs to be improved.

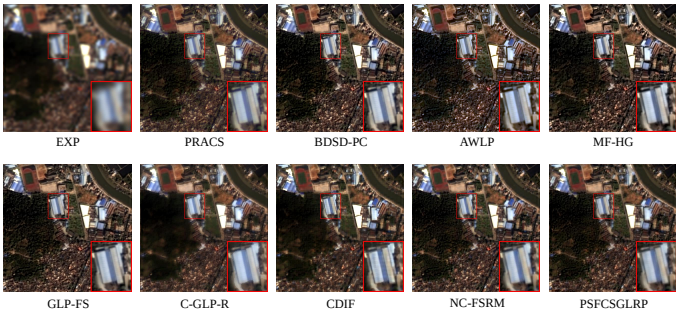

Fig. 4. The fusion results on the reduced-resolution Guangzhou dataset.

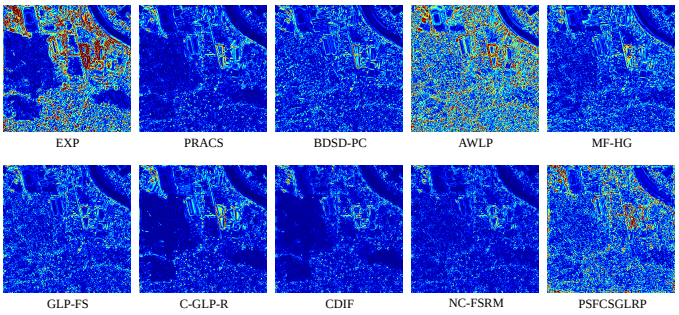

Fig. 5. The residuals of fusion results on the reduced-resolution Guangzhou dataset.

TABLE II
NUMERICAL RESULTS OF DIFFERENT METHODS

Method	PSNR	SSIM	SAM
EXP	38.0241 ± 1.9739	0.9177 ± 0.0288	1.817 ± 0.367
PRACS	41.3029 ± 1.8215	0.9605 ± 0.0129	1.6877 ± 0.3262
BDSD-PC	41.0471 ± 2.092	0.9574 ± 0.0164	1.696 ± 0.3252
AWLP	40.5613 ± 2.1045	0.9455 ± 0.0232	1.9332 ± 0.521
MF-HG	40.566 ± 1.9012	0.9554 ± 0.015	1.6462 ± 0.3304
GLP-FS	41.4236 ± 1.9558	0.9558 ± 0.0162	1.6553 ± 0.3524
C-GLP-R	41.3444 ± 1.8539	0.9652 ± 0.013	1.5589 ± 0.2944
CDIF	43.3541 ± 1.8838	0.9722 ± 0.0094	1.2758 ± 0.2538
NC-FSRM	43.2011 ± 1.9831	0.9692 ± 0.0112	1.3691 ± 0.3056
SFLR	41.7462 ± 1.6752	0.9646 ± 0.0124	1.4657 ± 0.3105

Method	SCC	ERGAS	Q4
EXP	0.9282 ± 0.0362	2.3563 ± 0.5006	0.8118 ± 0.0481
PRACS	0.9651 ± 0.0203	1.6244 ± 0.3587	0.9023 ± 0.0295
BDSD-PC	0.9655 ± 0.0178	1.6732 ± 0.4085	0.9011 ± 0.027
AWLP	0.961 ± 0.0187	1.6482 ± 0.3971	0.8814 ± 0.0316
MF-HG	0.9645 ± 0.016	1.7009 ± 0.3338	0.8919 ± 0.0269
GLP-FS	0.9661 ± 0.0176	1.5969 ± 0.3663	0.8969 ± 0.0284
C-GLP-R	0.9668 ± 0.0199	1.5434 ± 0.3696	0.9212 ± 0.0231
CDIF	0.9784 ± 0.0117	1.2633 ± 0.3031	0.9425 ± 0.0185
NC-FSRM	0.9759 ± 0.0147	1.2971 ± 0.3164	0.9337 ± 0.0213
SFLR	0.9724 ± 0.0153	1.4506 ± 0.3289	0.9242 ± 0.0212

V. CONCLUSION AND FUTURE WORK

A. Conclusion

In this paper, we constructed a new pansharpening model with spatial framelet consistency and spectral gradient low

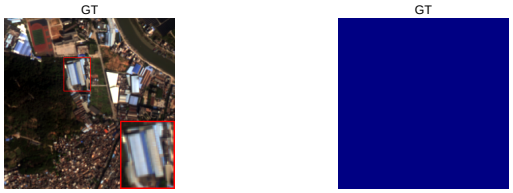

(a) (b)

Fig. 6. Ground truth and its residual.

rank priors. We used the similarity of HRMS and PAN in the framelet field, and proposed spatial framelet consistency term to improve the spatial similarity of reconstructed HRMS. And we used the spectral gradient low rank prior to ensure the gradient low rank feature of HRMS. Last, ADMM framework was used to solve the model. Experiments show the advantage of our methods to many traditional models, but they also show drawbacks compared with modern pansharpening frameworks.

B. Future Work

As known for all, the Deep Learning (DL) approaches for pan-sharpening excel in feature extraction and have a keen aptitude for learning nonlinear mappings, typically yielding impressive outcomes in image fusion. However, once a DL model is trained on data from a specific sensor, its parameters become rigidly aligned to that dataset, frequently prohibiting adaptation to new datasets from disparate sensors. [45] To improve the generalization ability of supervised DL methods, we aim to generalize the supervised DL methods in a variational fusion framework.

Meanwhile, the performance of our current model is not satisfactory, possibly due to unfitting of priors. So we can combine our model and DL approaches, which will raise the ability of our model to extract features. In paper [45], deep plug-and-play prior is used for pansharpening, and it has shown powerful effect. In our future work, we will design a new deep plug-and-play prior to improve current low rank prior. By harnessing deep learning techniques and ingeniously designed plug-and-play regularizers, we can refine variational optimization methods, leading to superior image fusion and broader applicability across varying datasets and sensors.

REFERENCES

[1] M. Zanetti, F. Bovolo, and L. Bruzzone, "Rayleigh-rice mixture parameter estimation via em algorithm for change detection in multispectral images," *IEEE Transactions on Image Processing*, vol. 24, no. 12, pp. 5004–5016, 2015.

[2] X. Yu, L. E. Hoff, I. S. Reed, A. M. Chen, and L. B. Stotts, "Automatic target detection and recognition in multiband imagery: A unified ml detection and estimation approach," *IEEE Transactions on Image Processing*, vol. 6, no. 1, pp. 143–156, 1997.

[3] P. Zhong and R. Wang, "Learning conditional random fields for classification of hyperspectral images," *IEEE transactions on image processing*, vol. 19, no. 7, pp. 1890–1907, 2010.

[4] Z.-C. Wu, T.-Z. Huang, L.-J. Deng, J. Huang, J. Chanussot, and G. Vivone, "Lrtcfpan: Low-rank tensor completion based framework for pansharpening," *IEEE Transactions on Image Processing*, vol. 32, pp. 1640–1655, 2023.

[5] P. Kwarteng and A. Chavez, "Extracting spectral contrast in landsat thematic mapper image data using selective principal component analysis," *Photogramm. Eng. Remote Sens*, vol. 55, no. 1, pp. 339–348, 1989.

[6] W. Carper, T. Lillesand, R. Kiefer *et al.*, "The use of intensity-hue-saturation transformations for merging spot panchromatic and multispectral image data," *Photogrammetric Engineering and remote sensing*, vol. 56, no. 4, pp. 459–467, 1990.

[7] B. Aiazzi, S. Baronti, and M. Selva, "Improving component substitution pansharpening through multivariate regression of ms + pan data," *IEEE Transactions on Geoscience and Remote Sensing*, vol. 45, no. 10, pp. 3230–3239, 2007.

[8] A. Garzelli, F. Nencini, and L. Capobianco, "Optimal mmse pan sharpening of very high resolution multispectral images," *IEEE Transactions on Geoscience and Remote Sensing*, vol. 46, no. 1, pp. 228–236, 2007.

[9] J. Choi, K. Yu, and Y. Kim, "A new adaptive component-substitution-based satellite image fusion by using partial replacement," *IEEE transactions on geoscience and remote sensing*, vol. 49, no. 1, pp. 295–309, 2010.

[10] M. J. Shensa *et al.*, "The discrete wavelet transform: wedding the a trous and mallat algorithms," *IEEE Transactions on signal processing*, vol. 40, no. 10, pp. 2464–2482, 1992.

[11] X. Otazu, M. González-Audícana, O. Fors, and J. Núñez, "Introduction of sensor spectral response into image fusion methods. application to wavelet-based methods," *IEEE Transactions on Geoscience and Remote Sensing*, vol. 43, no. 10, pp. 2376–2385, 2005.

[12] J. Liu, "Smoothing filter-based intensity modulation: A spectral preserve image fusion technique for improving spatial details," *International Journal of remote sensing*, vol. 21, no. 18, pp. 3461–3472, 2000.

[13] L.-J. Deng, G. Vivone, C. Jin, and J. Chanussot, "Detail injection-based deep convolutional neural networks for pansharpening," *IEEE Transactions on Geoscience and Remote Sensing*, vol. 59, no. 8, pp. 6995–7010, 2020.

[14] P. Addesso, G. Vivone, R. Restaino, and J. Chanussot, "A data-driven model-based regression applied to panchromatic sharpening," *IEEE Transactions on Image Processing*, vol. 29, pp. 7779–7794, 2020.

[15] Z.-R. Jin, L.-J. Deng, T.-J. Zhang, and X.-X. Jin, "Bam: Bilateral activation mechanism for image fusion," in *Proceedings of the 29th ACM international conference on multimedia*, 2021, pp. 4315–4323.

[16] Y. Wang, L.-J. Deng, T.-J. Zhang, and X. Wu, "Ssconv: Explicit spectral-to-spatial convolution for pansharpening," in *Proceedings of the 29th ACM international conference on multimedia*, 2021, pp. 4472–4480.

[17] X. Fu, W. Wang, Y. Huang, X. Ding, and J. Paisley, "Deep multiscale detail networks for multiband spectral image sharpening," *IEEE Transactions on Neural Networks and Learning Systems*, vol. 32, no. 5, pp. 2090–2104, 2020.

[18] X. Lu, J. Zhang, D. Yang, L. Xu, and F. Jia, "Cascaded convolutional neural network-based hyperspectral image resolution enhancement via an auxiliary panchromatic image," *IEEE Transactions on Image Processing*, vol. 30, pp. 6815–6828, 2021.

[19] X. Fu, Z. Lin, Y. Huang, and X. Ding, "A variational pan-sharpening with local gradient constraints," in *Proceedings of the IEEE/CVF Conference on Computer Vision and Pattern Recognition*, 2019, pp. 10 265–10 274.

[20] C. Ballester, V. Caselles, L. Igual, J. Verdera, and B. Rougé, "A variational model for p+ xs image fusion," *International Journal of Computer Vision*, vol. 69, pp. 43–58, 2006.

[21] Y. Jiang, X. Ding, D. Zeng, Y. Huang, and J. Paisley, "Pan-sharpening with a hyper-laplacian penalty," in *Proceedings of the IEEE International Conference on Computer Vision*, 2015, pp. 540–548.

[22] T. Wang, F. Fang, F. Li, and G. Zhang, "High-quality bayesian pansharpening," *IEEE Transactions on Image Processing*, vol. 28, no. 1, pp. 227–239, 2018.

[23] L.-J. Deng, G. Vivone, W. Guo, M. Dalla Mura, and J. Chanussot, "A variational pansharpening approach based on reproducible kernel hilbert space and heaviside function," *IEEE Transactions on Image Processing*, vol. 27, no. 9, pp. 4330–4344, 2018.

[24] A. M. Teodoro, J. M. Bioucas-Dias, and M. A. Figueiredo, "A convergent image fusion algorithm using scene-adapted gaussian-mixture-based denoising," *IEEE Transactions on Image Processing*, vol. 28, no. 1, pp. 451–463, 2018.

[25] L.-J. Deng, M. Feng, and X.-C. Tai, "The fusion of panchromatic and multispectral remote sensing images via tensor-based sparse modeling and hyper-laplacian prior," *Information Fusion*, vol. 52, pp. 76–89, 2019.

[26] Z.-C. Wu, T.-Z. Huang, L.-J. Deng, G. Vivone, J.-Q. Miao, J.-F. Hu, and X.-L. Zhao, "A new variational approach based on proximal deep injection and gradient intensity similarity for spatio-spectral image fusion," *IEEE Journal of Selected Topics in Applied Earth Observations and Remote Sensing*, vol. 13, pp. 6277–6290, 2020.

[27] Y. Chen, T.-Z. Huang, X.-L. Zhao, and L.-J. Deng, "Hyperspectral image restoration using framelet-regularized low-rank nonnegative matrix factorization," *Applied Mathematical Modelling*, vol. 63, pp. 128–147, 2018.

[28] T.-X. Jiang, T.-Z. Huang, X.-L. Zhao, T.-Y. Ji, and L.-J. Deng, "Matrix factorization for low-rank tensor completion using framelet prior," *Information Sciences*, vol. 436, pp. 403–417, 2018.

[29] Y. Chang, H. Fang, L. Yan, and H. Liu, "Robust destriping method with unidirectional total variation and framelet regularization," *Optics express*, vol. 21, no. 20, pp. 23 307–23 323, 2013.

[30] P. Liu, "Pansharpening with spatial hessian non-convex sparse and spectral gradient low rank priors," *IEEE Transactions on Image Processing*, vol. 32, pp. 2120–2131, 2023.

[31] W. Zuo, D. Meng, L. Zhang, X. Feng, and D. Zhang, "A generalized iterated shrinkage algorithm for non-convex sparse coding," in *Proceedings of the IEEE international conference on computer vision*, 2013, pp. 217–224.

[32] J.-F. Cai, E. J. Candès, and Z. Shen, "A singular value thresholding algorithm for matrix completion," *SIAM Journal on optimization*, vol. 20, no. 4, pp. 1956–1982, 2010.

[33] L. Wald, T. Ranchin, and M. Mangolini, "Fusion of satellite images of different spatial resolutions: Assessing the quality of resulting images," *Photogrammetric engineering and remote sensing*, vol. 63, no. 6, pp. 691–699, 1997.

[34] B. Aiazzi, L. Alparone, S. Baronti, and A. Garzelli, "Context-driven fusion of high spatial and spectral resolution images based on oversampled multiresolution analysis," *IEEE Transactions on geoscience and remote sensing*, vol. 40, no. 10, pp. 2300–2312, 2002.

[35] J. Choi, K. Yu, and Y. Kim, "A new adaptive component-substitution-based satellite image fusion by using partial replacement," *IEEE transactions on geoscience and remote sensing*, vol. 49, no. 1, pp. 295–309, 2010.

[36] G. Vivone, "Robust band-dependent spatial-detail approaches for panchromatic sharpening," *IEEE transactions on Geoscience and Remote Sensing*, vol. 57, no. 9, pp. 6421–6433, 2019.

[37] X. Otazu, M. González-Audícana, O. Fors, and J. Núñez, "Introduction of sensor spectral response into image fusion methods. application to wavelet-based methods," *IEEE Transactions on Geoscience and Remote Sensing*, vol. 43, no. 10, pp. 2376–2385, 2005.

[38] R. Restaino, G. Vivone, M. Dalla Mura, and J. Chanussot, "Fusion of multispectral and panchromatic images based on morphological operators," *IEEE Transactions on Image Processing*, vol. 25, no. 6, pp. 2882–2895, 2016.

[39] G. Vivone, R. Restaino, and J. Chanussot, "Full scale regression-based injection coefficients for panchromatic sharpening," *IEEE Transactions on Image Processing*, vol. 27, no. 7, pp. 3418–3431, 2018.

[40] G. Vivone, S. Marano, and J. Chanussot, "Pansharpening: Context-based generalized laplacian pyramids by robust regression," *IEEE Transactions on Geoscience and Remote Sensing*, vol. 58, no. 9, pp. 6152–6167, 2020.

[41] X. Fu, Z. Lin, Y. Huang, and X. Ding, "A variational pan-sharpening with local gradient constraints," in *Proceedings of the IEEE/CVF Conference on Computer Vision and Pattern Recognition*, 2019, pp. 10 265–10 274.

[42] L.-J. Deng, M. Feng, and X.-C. Tai, "The fusion of panchromatic and multispectral remote sensing images via tensor-based sparse modeling and hyper-laplacian prior," *Information Fusion*, vol. 52, pp. 76–89, 2019.

[43] J.-L. Xiao, T.-Z. Huang, L.-J. Deng, Z.-C. Wu, and G. Vivone, "A new context-aware details injection fidelity with adaptive coefficients estimation for variational pansharpening," *IEEE Transactions on Geoscience and Remote Sensing*, vol. 60, pp. 1–15, 2022.

[44] Z.-C. Wu, T.-Z. Huang, L.-J. Deng, and G. Vivone, "A framelet sparse reconstruction method for pansharpening with guaranteed convergence," *Inverse Problems and Imaging*, vol. 17, no. 6, pp. 1277–1300, 2023.

[45] P. Liu, J. Liu, and L. Xiao, "A unified pansharpening method with structure tensor driven spatial consistency and deep plug-and-play priors," *IEEE Transactions on Geoscience and Remote Sensing*, vol. 60, pp. 1–14, 2022.